Science
AAAS

Controlled Formation of Sharp Zigzag and Armchair Edges in Graphitic Nanoribbons

Xiaoting Jia, *et al.*

Science **323**, 1701 (2009);
DOI: 10.1126/science.1166862

Science (print ISSN 0036-8075; online ISSN 1095-9203) is published weekly, except the last week in December, by the American Association for the Advancement of Science, 1200 New York Avenue NW, Washington, DC 20005.

lubrication between articular cartilage surfaces. Biological lubrication at such synovial joints, despite many decades of study, is not yet well understood at the molecular level (*29*–*31*). Recent models have focused on the role of pressurized interstitial water (*31*) and of macromolecules at the outer cartilage surface (*30*). Our system of synthetic polyzwitterionic brushes polymerized from molecularly smooth mica surfaces does not have a clear analog at the cartilage surface, at which macromolecular components of the cartilage and the synovial fluid surrounding it are likely to be present [including proteins, hyaluronic acid, proteoglycans, glycoproteins, and lipidic molecules (*30*)]. The detailed role of these in the lubrication process, as well as of the cartilage substrate itself, has yet to be clarified. Moreover, cartilage is softer and much rougher than mica, though at these high pressures it may deform affinely (*30*); experiments on similarly soft and roughened brush-coated surfaces could potentially provide insight into the mechanisms that are operative in cartilage-cartilage friction. The highly hydrated PC-like monomers on our pMPC chains provide very efficient lubrication. The structure of these is similar to that of lipid headgroups, which provides some context for the recent controversial suggestion that lipid multilayers may have a role in mediating synovial lubrication (*29*), particularly in view of recent findings on the mechanism of boundary lubrication under water (*11*). Finally, although our polyzwitterionic brushes have no direct analog at cartilage surfaces, our results underline the possible importance at such surfaces of highly hydrated macromolecules in both chondroprotective and lubrication roles.

We have shown that brushes of a biocompatible polyzwitterion, pMPC, are capable of providing extremely efficient lubrication in aqueous media with coefficients of friction $\mu \approx 0.001$ at mean pressures up to 7.5 MPa, which are comparable to values in human synovial joints. We attribute the low friction at the high pressure primarily to the lubricating action of tenaciously attached but labile water molecules about the strongly hydrated MPC monomers. Our results may have relevance for boundary lubrication in human-made systems in aqueous or physiological media, as in biomedical devices, in which friction and wear are often an issue.

References and Notes

1. C. W. McCutchen, *Fed. Proc.* **25**, 1061 (1966).
2. D. Swann, K. J. Bloch, D. Swindell, E. Shore, *Arthritis Rheum.* **27**, 552 (1984).
3. A. N. M. Forster, J. W. Mays, S. M. Kilbey, *J. Polym. Sci. Part B Polym. Phys.* **44**, 649 (2006).
4. J. Klein, E. Kumacheva, D. Mahalu, D. Perahia, L. Fetters, *Nature* **370**, 634 (1994).
5. U. Raviv *et al.*, *Nature* **425**, 163 (2003).
6. P. Schorr, T. Kwan, M. Kilbey, S. G. Shaqfeh, M. Tirrell, *Macromolecules* **36**, 389 (2003).
7. J. P. Gong *et al.*, *J. Am. Chem. Soc.* **123**, 5582 (2001).
8. D. Gourdon *et al.*, *Langmuir* **24**, 1534 (2008).
9. S. Lee, N. D. Spencer, *Science* **319**, 575 (2008).
10. U. Raviv, J. Klein, *Science* **297**, 1540 (2002).
11. W. H. Briscoe *et al.*, *Nature* **444**, 191 (2006).
12. Materials and methods are available as supporting material on *Science* Online.
13. M. Chen, W. H. Briscoe, S. P. Armes, H. Cohen, J. Klein, *ChemPhysChem* **8**, 1303 (2007).
14. J. Klein, E. Kumacheva, *J. Chem. Phys.* **108**, 6996 (1998).
15. This robustness is consistent with the nature of the pMPC brushes' attachment to the mica and the shear forces applied. For an area per macroinitiator $A_m \approx 16$ nm^2 (*13*) and a mean pressure P, the shear force acting on a single macroinitiator molecule [$F_{s(m)}$] through the chains growing from it is given by $F_{s(m)} = \mu P A_m$. Because the chains are attached covalently to the initiation sites, any detachment due to shear is expected to commence at the weaker bonds attaching the macroinitiator to the mica. These bonds (on average ~18 such bonds per macroinitiator) each have a net adhesion energy $\varepsilon_1 \approx k_B T$ (k_B is the Boltzmann constant and T is the temperature) arising from replacement of counterions at the negatively charged mica surface by the positively charged quaternary $-N^+(CH_3)_3$ groups on the macroinitiator. In the worst-case scenario, all the $F_{s(m)}$ during sliding will act on one of the quaternary groups at the surface, and this may initiate the "unzipping" of the macroinitiator from the mica. Putting $\mu = 0.001$ and $P = 7.5$ MPa gives $F_{s(m)} = 1.2 \times 10^{-13}$ N. This is smaller than the force $f_1 \approx \varepsilon_1/\delta$ that is needed to detach a single $-N^+(CH_3)_3$ group from the mica, where δ is on the order of 1 Å or less. Putting $\delta = 1$ Å gives $f_1 \approx 4 \times 10^{-11}$ N. Thus, the friction force on a macroinitiator at the highest pressures we apply is too weak (by a factor of 100 or more) to detach even a single bond anchoring the macroinitiator to the mica surface, which is consistent with our observations of the robustness of the pMPC layer toward resisting shear under all conditions in our study.
16. T. Witten, L. Leibler, P. Pincus, *Macromolecules* **23**, 824 (1990).
17. R. Tadmor, J. Janik, L. J. Fetters, J. Klein, *Phys. Rev. Lett.* **91**, 115503 (2003).
18. E. A. Disalvo *et al.*, *J. Argent. Chem. Soc.* **92**, 1 (2004).
19. M. Yaseen, J. R. Lu, *Langmuir* **22**, 5825 (2006).
20. G. Pabst, M. Rappolt, H. Amenitsch, P. Laggner, *Phys. Rev. E Stat. Phys. Plasmas Fluids Relat. Interdiscip. Topics* **62**, 4000 (2000).
21. J. F. Nagle *et al.*, *Biophys. J.* **70**, 1419 (1996).
22. K. Ishihara *et al.*, *J. Biomed. Mater. Res.* **39**, 323 (1998).
23. L. J. Lis, M. McAlister, N. Fuller, R. P. Rand, V. A. Parsegian, *Biophys. J.* **37**, 657 (1982).
24. W. Feng *et al.*, *Biointerphases* **2**, 34 (2007).
25. F. A. Cotton, G. Wilkinson, *Advanced Inorganic Chemistry* (Wiley, New York, ed. 5, 1998), pp. 1288–1289.
26. M. Rappolt, G. Pabst, H. Amenitsch, P. Laggner, *Colloids Surf. A Physicochem. Eng. Asp.* **183-185**, 171 (2001).
27. T. Moro *et al.*, *Nat. Mater.* **3**, 829 (2004).
28. M. Kobayashi *et al.*, *Soft Matter* **3**, 740 (2007).
29. B. A. Hills, G. D. Jay, *J. Rheumatol.* **29**, 200 (2002).
30. J. Klein, *Proc. Inst. Mech. Eng. Part J J. Eng. Tribol.* **220**, 691 (2006).
31. S. Park, K. D. Costa, G. A. Ateshian, *J. Biomech.* **37**, 1679 (2004).
32. D. Y. C. Chan, R. M. Pashley, L. R. White, *J. Colloid Interface Sci.* **77**, 283 (1980).

33. We thank A. L. Lewis (Biocompatibles Ltd.) for kind donation of the MPC monomer; X. Y. Chen for synthesis of the macroinitiator; I. E. Dunlop, S. Perkin, and W. Feng for help and advice; and P. Pincus for a discussion. S.P.A. is the recipient of a Royal Society Research Merit Award. W.H.B. thanks the Taiho Kogyo Tribology Research Foundation for support. This work was supported by the Engineering and Physical Sciences Research Council, the Petroleum Research Fund (grant 45694-AC7), the Charles McCutchen Foundation, and the Minerva Foundation at the Weizmann Institute.

Supporting Online Material

www.sciencemag.org/cgi/content/full/323/5922/1698/DC1
Materials and Methods
References

5 December 2008; accepted 21 January 2009
10.1126/science.1169399

Controlled Formation of Sharp Zigzag and Armchair Edges in Graphitic Nanoribbons

Xiaoting Jia,[1] Mario Hofmann,[2] Vincent Meunier,[3] Bobby G. Sumpter,[3] Jessica Campos-Delgado,[4] José Manuel Romo-Herrera,[4] Hyungbin Son,[2] Ya-Ping Hsieh,[2] Alfonso Reina,[1] Jing Kong,[2] Mauricio Terrones,[4] Mildred S. Dresselhaus[2,5]*

Graphene nanoribbons can exhibit either quasi-metallic or semiconducting behavior, depending on the atomic structure of their edges. Thus, it is important to control the morphology and crystallinity of these edges for practical purposes. We demonstrated an efficient edge-reconstruction process, at the atomic scale, for graphitic nanoribbons by Joule heating. During Joule heating and electron beam irradiation, carbon atoms are vaporized, and subsequently sharp edges and step-edge arrays are stabilized, mostly with either zigzag- or armchair-edge configurations. Model calculations show that the dominant annealing mechanisms involve point defect annealing and edge reconstruction.

Graphene, a single sheet of graphite, has attracted a lot of research interest since it first became experimentally accessible in 2004 (*1*–*5*). Its two-dimensional (2D) structure and the near massless behavior of its charge carriers provide unique transport properties. Graphene nanoribbons, which are quasi-1D graphene nanostructures, exhibit a bandgap between the valence and conduction band states. The bandgap depends on both the edge type and ribbon width (*6*), which is typically a few nanometers, making graphene nanoribbons a very interesting material for potential electronics applications (*7*). Theoretical and experimental studies show that the edges of graphene nanoribbons strongly influence their electronic and magnetic properties (*8*, *9*). Therefore, much effort has been devoted to studying the edges in graphitic nanomaterials (*10*–*18*). Although atomically smooth edges are essential for many applications, it is difficult to produce such edges by conventional physico-chemical methods. For example, lithographic etching and

chemical methods usually provide rough edges (*19*) that contribute to carrier scattering. Furthermore, characterizing the edges and identifying the edge structure has been a challenge.

With an integrated transmission electron microscope–scanning tunneling microscope (TEM-STM) system [see supporting online material (SOM)], we are able to produce atomically smooth zigzag or armchair edges from defective rough edges that are observed in specially prepared graphitic nanoribbons (*20*). The graphitic nanoribbon samples are produced by a chemical vapor deposition process (*20*), as summarized in the SOM (fig. S1A). An individual nanoribbon sample is attached to the sample holder at one end and to the STM tip at the other end; these ends also serve as the two electrodes. As we apply a voltage (up to 1.6 V) over the length (315 nm) of a 66-nm-wide ribbon, the current (*I*)–versus–voltage (*V*) curve shows (Fig. 1A) the onset of a nonlinear regime (at 1.6 V), where the resistance decreases with increasing input energy (Fig. 1B). As current flows, the degree of crystallinity of the ribbon improves rapidly (Fig. 1, C and D), and the sample thickness decreases, until all the graphene layers evaporate and the sample breaks from the middle (fig. S1B). From the edge terminations observed in Fig. 1E, we conclude that the majority of edges are either zigzag or armchair after Joule heating.

It is important to note that in the lower voltage (quasi-linear) regime below 1.6 V (see Fig. 1A), carbon atoms mainly vaporize because of knock-on effects caused by the electron irradiation (*21*), and edges start reconstructing via Joule annealing. However, at higher applied voltages (1.6 V), the preferred reconstruction-crystallization effects induced by the high temperature caused by Joule heating are seen in going from Fig. 1, C to D, indicating that the activation energy of atoms forming zigzag or armchair edges is lower than for other edge configurations. Other types of edges are seen infrequently because a mixture of zigzag and armchair edges is metastable due to an energy penalty at the edge junctions. Figure 1F depicts the reconstructed graphitic material shown in Fig. 1D. The measured in-plane lattice spacing for our ribbons is 0.24 ± 0.02 nm, consistent (within the accuracy of our TEM measurements) with literature values for graphite [which is $\sqrt{3}a_{c-c}$, where a_{c-c} is the nearest-neighbor carbon-to-carbon distance (*22*)]. As a result of carbon atom vaporization and Joule heating, the defective graphitic edges in the as-grown nanoribbon sample crystallize (fig. S2) and finally become atomically sharp and highly crystalline. The maximum length of the smooth edges observed after the process in Fig. 1E is ~29 nm. The mechanism of reconstruction or crystallization for the nanoribbons and edges is attributed primarily to the carbon atom vaporization, the current flow along the ribbon and edges, and the high temperature associated with the resistive Joule heating (see SOM).

The graphitization steps of carbon at high temperatures have been described by Goma and Oberlin (*23*, *24*). Here the graphitization process culminates in the thermal crystallization of wavy and wrinkled layers into long in-plane crystalline domains by ~2100°C with *c*-axis stacking order starting to develop above 2300°C and identified with crystalline graphite. For our ribbon samples, we observed the transformation of AA stacking into ABAB stacking, and we attribute these transformations mainly to the high temperatures reached (above 2000°C) in the nonlinear voltage regime. To verify that a high temperature is achieved by

[1]Department of Materials Science and Engineering, Massachusetts Institute of Technology, Cambridge, MA 02139–4307, USA. [2]Department of Electrical Engineering and Computer Science, Massachusetts Institute of Technology, Cambridge, MA 02139–4307, USA. [3]Computer Science and Mathematics Division and Center for Nanophase Materials Sciences, Oak Ridge National Laboratory (ORNL), Post Office Box 2008, Oak Ridge, TN 37831–6367, USA. [4]Laboratory for Nanoscience and Nanotechnology Research (LINAN) and Advanced Materials Department, Instituto Potosino de Investigación Científica y Tecnológica, Camino a la Presa San José 2055, Col. Lomas 4a. sección, San Luis Potosí 78216, México. [5]Department of Physics, Massachusetts Institute of Technology, Cambridge, MA 02139–4307, USA.

*To whom correspondence should be addressed. E-mail: millie@mgm.mit.edu

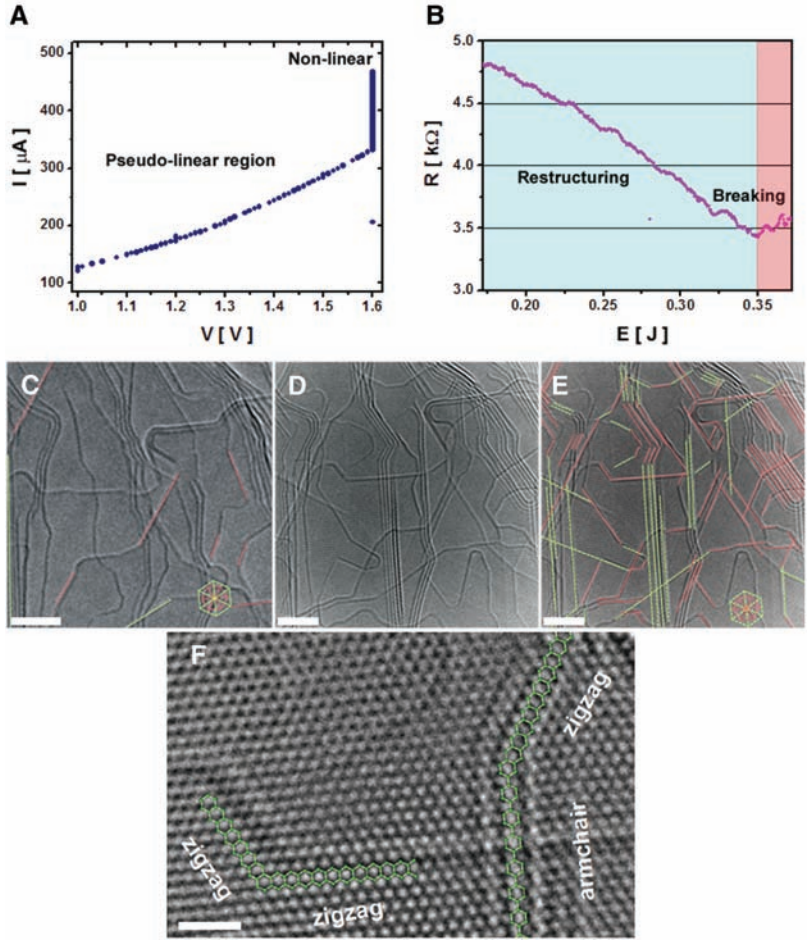

Fig. 1. Crystallization and edge formation in graphitic nanoribbons. (**A**) *I* versus *V* curve during Joule heating, indicating three regimes: (i) a linear regime from 1 to 1.25 V, (ii) a slowly increasing slope regime from 1.25 to 1.6 V, and (iii) a rapidly increasing slope regime at 1.6 V. (**B**) Resistance versus input energy at 1.6 V applied bias. (**C**) Ribbon sample before Joule heating, showing very few zigzag (pink lines) and armchair edges (green lines). (**D**) The same ribbon sample after Joule heating (for 10 min at 1.6 V), in which most of the edges seen are either zigzag or armchair edges, as indicated in (**E**). The inset hexagons indicate the zigzag- or armchair-edge orientations associated with the lattice patterns in (C) and (E). (**F**) High-magnification image of the annealed sample showing that well-defined zigzag-armchair and zigzag-zigzag edges are formed. The green hexagons in (E) help with the identification of the atomic structure at the armchair and zigzag edges. Scale bars in (C), (D) and (E), 4 nm; in (F), 1 nm.

resistive Joule heating in the suspended graphitic nanoribbons, Pt nanoparticles were deposited on an as-prepared ribbon (fig. S4). Upon Joule heating (with an applied bias below 2V), the Pt nanoparticles evaporate from the center region of the nanoribbon surface (fig. S5), thus indicating that a high temperature is achieved by Joule heating along the freely suspended ribbon (see SOM).

The dynamics of the edge reconstruction are shown in Fig. 2, A to D, and fig. S3. In Fig. 2, A to D, we see a time resolved sequence of a three-layered graphene edge structure placed on top of another few-layered graphene sheet with a zigzag-armchair-zigzag-armchair edge configuration forming 150° angles (note that the angles between zigzag and armchair edges can be 30°, 90°, or 150°). As we apply a bias voltage of 1.6 V (high annealing temperatures), the armchair edge above the zigzag edge starts to evaporate, resulting in the upward movement of the zigzag edge (red arrows) with a speed of 2.3 nm/min. This low speed at the investigated high temperatures indicates that the necessary activation energy is much larger than the activation energy of defect migration observed by Jin *et al.* (*25*) in carbon nanotubes. Eventually, as shown in Fig. 2D, the armchair edge is eliminated, and the lower zigzag edge joins with the upper zigzag edge and forms a stable zigzag-zigzag junction.

In Fig. 2E, the edge motion direction and speed are plotted for 14 experiments over the

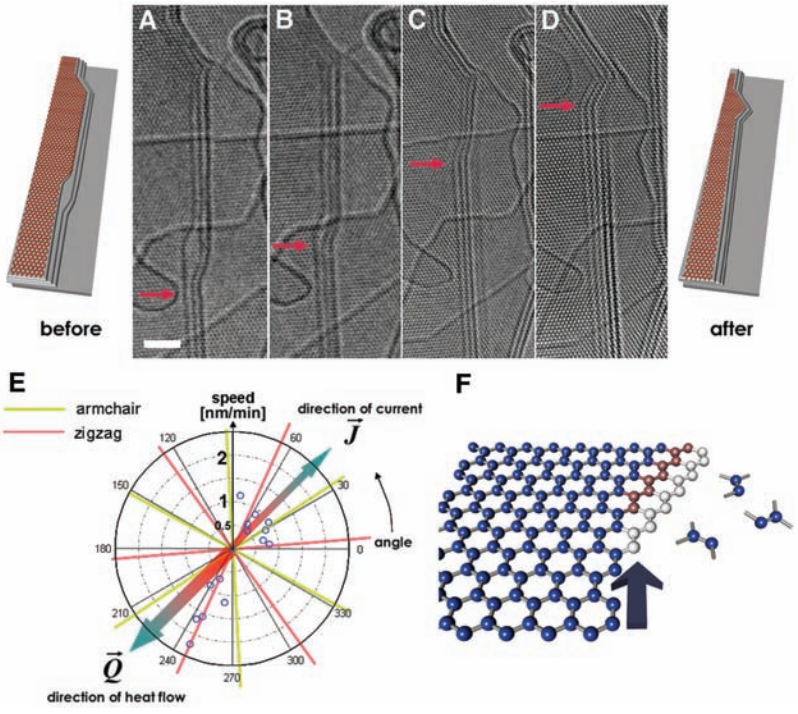

Fig. 2. Edge motion under Joule heating inside the TEM. (**A**) Three-layer zigzag-armchair-zigzag-armchair edge array. The red arrow indicates the position of the zigzag-armchair edge junction at the beginning of the annealing process. After some time of Joule heating, the junction moves up [(**B**) and (**C**)], keeping the short zigzag-edge length almost unchanged. Eventually, the zigzag edge joins with the upper zigzag edge, forming a stable zigzag-zigzag-armchair edge array (**D**). The sketches on the left of (A) and on the right of (D) are the simulated structures of (A) and (D), respectively. (**E**) Plot of the speed (in the radial direction) and angle (in the counterclockwise direction) of the edge motion relative to the current and heat flow directions. (**F**) A scenario for the motion of carbon atoms near edges and edge junctions, as C_2 dimers are evaporated from edges. As a row of the carbon atoms near the zigzag edge move away from the edge (first white colored balls and then red colored balls) upon heating, the zigzag-armchair edge junction (indicated by a black arrow) moves upward by $3a_{c\text{-}c}$. Scale bar in (A), 2 nm.

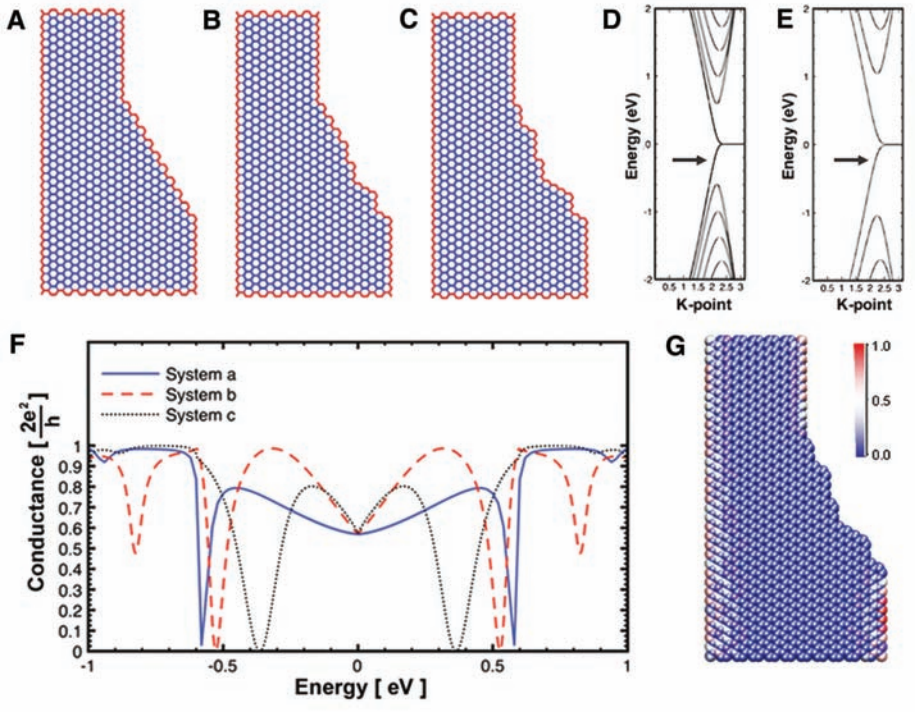

Fig. 3. Electronic and transport properties of graphene nanoribbon heterojunctions based on a single π-orbital tight-binding model (the Fermi energy is located at $E = 0$ eV). (**A** to **C**) Three models considered here where the details of the edges are highlighted in red. In each case, the two electrodes consist of two zigzag-edge nanoribbons [$N_{zig} = 44$ and 24, using notation from (*29*)]. The electronic properties of the individual electrodes are represented in (**D**) and (**E**) for the large and small ribbons, respectively. The conductance corresponding to systems (A) to (C) is presented in (**F**). For system (C), the amplitude of the scattered wave function (current-carrying state) is shown in (**G**); it is normalized such that the maximum amplitude is 1. The figure in (G) confirms that, close to the Fermi level, the current-carrying state in the zigzag taper is localized along the zigzag edges (zero amplitude at the inner part of the figure) and that the tapered part of the junction presents a high electrical resistance.

ribbon sample, similar to that shown in Fig. 2, A to D. From Fig. 2E, we see that the edge motion mostly follows either zigzag or armchair crystallographic orientations, and that the speed of edges moving along the heat flow direction $\vec{Q}$ (from the middle of the ribbon to the two electrodes acting as heat sinks) is higher (2 nm/min) than that along the current flow direction $\vec{J}$ (from the STM probe to the sample holder) when the two are antiparallel (1 nm/min). Edge motion along other directions is not favored. A scenario for the dissociation of carbon atoms from edges and the resulting motion of the edge junctions is given in Fig. 2F.

The reason why thermal energy is dissipated at an edge hetero-junction is because it is the location of the largest electrical resistance. Therefore, quasi-metallic [zigzag-edged or one-third of armchair-edged graphene nanoribbons (*26*)] systems should be preferred. Joule heating involves both current flow and atomic vibrations. Carbon nanoribbons do not show any specific phonon associated with a given edge type (there is no special phonon localized on the edges themselves) (*27*). Point (localized) defects are associated with large amplitude vibrations, and these are likely to be annealed first. In addition, zigzag-edged graphene ribbons are the only graphene structures which have electronic states that are localized along their edges (*9*). Because the electronic dispersion is quite large (Fig. 3, D and E), the electronic flow in zigzag-edged nanoribbons occurs mainly along these zigzag edges. When a zigzag edge meets a non-zigzag edge, the electronic flow is reduced, and the system acts as if a large resistance were introduced at the junction. Therefore, heating will result and will cause electron flow away from the edge junction or, if enough energy is dissipated at the junction, will result in a modification of the structure. In that case, provided that sufficient energy is dissipated in this manner, the atomic structure will rearrange locally (fig. S6) until electronic flow is reestablished. Starting from a zigzag edge, this can take place if the structure is annealed into a zigzag edge. For this reason, zigzag-zigzag junctions are the favored junction formation (Fig. 1). This zigzag edge formation mechanism is therefore local, because it is due to a high local resistance at the edge intersection.

To verify this hypothesis, we considered the three junctions shown in Fig. 3, A to C, which differ in the structure of the tapered edge: In Fig. 3A, the junction is made by an armchair edge, whereas the junctions in Fig. 3, B and C, are a mixture of edge geometries. The conductance of the hetero-junctions between zigzag and armchair edges is considerably reduced because of the fact that transmission is hindered on those non-zigzag edges where no electronic state is present. The scattering amplitude of a current-carrying state close to E = 0 eV is shown in Fig. 3G, highlighting the appearance of a large, localized resistance where the zigzag edge is interrupted. In turn, this resistance results in local heating and subsequent annealing into an all–zigzag edge system.

A nonlocal transformation mechanism can be invoked to account for the formation of semimetallic conducting armchair edges. For larger current flow, the structure can also anneal into a conducting armchair-edge system, as the current is allowed to flow, albeit not along the edges themselves. The effect is nonlocal in nature because, even though the edge structure governs the semi-metallicity of the whole structure, the current flow in the nonlocal case mostly appears away from the edges.

Experimentally, we found that more zigzag edges are initially formed at high temperatures, which is an indication that local processes are dominant. Conversely, armchair-edged ribbons, although found in less abundance, are considerably longer (Figs. 1 and 2), lending support to an operative nonlocal mechanism. Also, it is important to note that armchair edges evaporate easily when compared with the zigzag edges (Fig. 2). Molecular dynamics calculations (fig. S6) show that a C–C unit located at the armchair edge dissociates preferentially; the energy required to vaporize a C–C unit from the armchair edge is 6.7 eV, whereas that of a zigzag edge is considerably higher (~11 eV).

The Joule annealing process and its associated current flow create stable "edge arrays" (see Fig. 1D and Fig. 2, A to D). These edge arrays indicate that an offset is present between the edges of two adjacent layers. The results of a careful measurement of the edge-to-edge distances in these edge arrays is plotted in Fig. 4A, which shows clear peaks at 0.34-, 0.38-, and 0.43-nm edge-to-edge distances. These distances correspond to the offset of adjacent edges of differently stacked graphene layers (Fig. 4A). Of particular interest, the evolution of the edge arrays (Fig. 4B) after 10 min of irradiation and Joule annealing shows a clear increase for the AB stacked zigzag edges and a decrease of the AA stacked zigzag edges. This observation is attributed to the fact that the ABAB stacked configuration is thermodynamically more stable than AA stacking (*28*) and is consistent with the Goma-Oberlin mechanism (*23*).

We demonstrated the efficient shaping of graphitic nanoribbon edges into zigzag or armchair edges via Joule heating inside a TEM-STM system. This structural transformation is mainly attributed to the vaporization of carbon edges that reconstruct at high temperatures, in which the resistive Joule heating and the preferred current flow along specific edges play a vital role. The theoretical edge evolution model reveals that the specific edge formation is stimulated as a means to provide an easy path for current flow between intersecting zigzag and conducting armchair edges. This means that the efficient formation of all zigzag-edge ribbons could be achieved by careful limitation of the flowing current. These results open up a possible

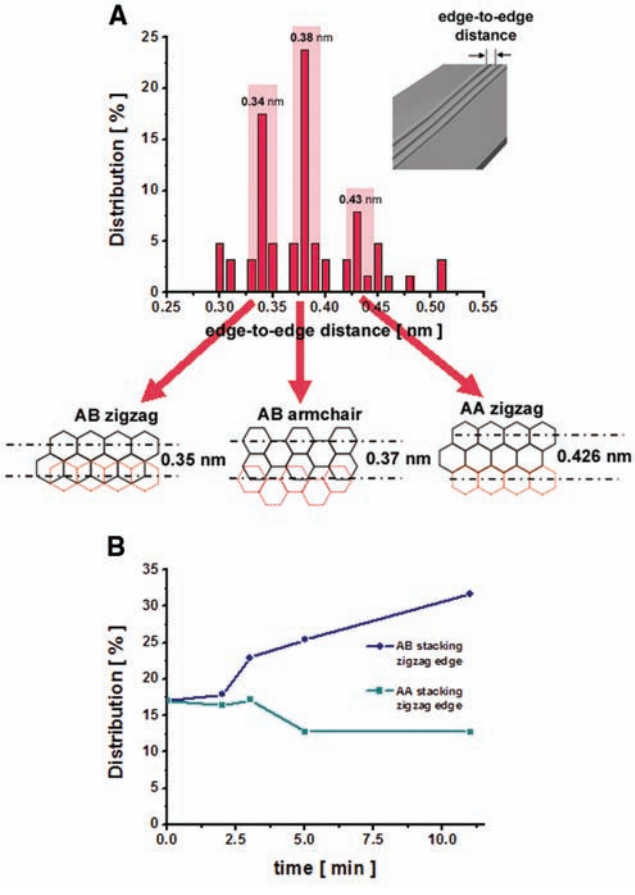

Fig. 4. Edge arrays and their time evolution. (**A**) The experimental edge-to-edge distances in the edge arrays show three peaks at 0.34, 0.38, and 0.43 nm. These peaks correspond to the offset of two adjacent AB stacked zigzag edges, AB stacked armchair edges, and AA stacked zigzag edges, respectively, as indicated in the inset of (A). (**B**) Of all the edges obtained from analysis of Fig. 1D, the percentage of AB stacked zigzag edges increases from 17 to 32%, whereas the percentage of AA stacked zigzag edges decreases from 17 to 13% after a 10-min anneal, indicating that the AB stacked layer configuration is more stable than AA stacking. Error of points is 2%.

way of generating atomically well-defined edges that make graphene-based electronics possible.

References and Notes

1. K. S. Novoselov *et al.*, *Science* **306**, 666 (2004).
2. K. S. Novoselov *et al.*, *Proc. Natl. Acad. Sci. U.S.A.* **102**, 10451 (2005).
3. Y. Zhang, Y. W. Tan, H. L. Stormer, P. Kim, *Nature* **438**, 201 (2005).
4. J. C. Meyer *et al.*, *Nature* **446**, 60 (2007).
5. A. K. Geim, K. S. Novoselov, *Nat. Mater.* **6**, 183 (2007).
6. Y. W. Son, M. L. Cohen, S. G. Louie, *Nature* **444**, 347 (2006).
7. X. Li, X. Wang, L. Zhang, S. Lee, H. Dai, *Science* **319**, 1229 (2008); published online 23 January 2008 (10.1126/science.1150878).
8. T. Enoki, Y. Kobayashi, K. Fukui, *Int. Rev. Phys. Chem.* **26**, 609 (2007).
9. K. Nakada, M. Fujita, G. Dresselhaus, M. S. Dresselhaus, *Phys. Rev. B* **54**, 17954 (1996).
10. K. Wakabayashi, *Phys. Rev. B* **64**, 125428 (2001).
11. L. G. Cançado *et al.*, *Phys. Rev. Lett.* **93**, 047403 (2004).
12. L. G. Cançado, M. A. Pimenta, B. R. A. Neves, M. S. S. Dantas, A. Jorio, *Phys. Rev. Lett.* **93**, 247401 (2004).
13. P. Shemella, Y. Zhang, M. Mailman, P. M. Ajayan, S. K. Nayak, *Appl. Phys. Lett.* **91**, 042101 (2007).
14. L. Yang, C. H. Park, Y. W. Son, M. L. Cohen, S. G. Louie, *Phys. Rev. Lett.* **99**, 186801 (2007).
15. X. Wang *et al.*, *Phys. Rev. Lett.* **100**, 206803 (2008).
16. T. C. Li, S. P. Lu, *Phys. Rev. B* **77**, 085408 (2008).
17. F. Cervantes-Sodi, G. Csányi, S. Piscanec, A. C. Ferrari, *Phys. Rev. B* **77**, 165427 (2008).
18. L. Tapasztó, G. Dobrik, P. Lambin, L. P. Biró, *Nat. Nanotechnol.* **3**, 397 (2008).
19. M. Y. Han, B. Özyilmaz, Y. Zhang, P. Kim, *Phys. Rev. Lett.* **98**, 206805 (2007).
20. J. Campos-Delgado *et al.*, *Nano Lett.* **8**, 2773 (2008).
21. F. Banhart, *Rep. Prog. Phys.* **62**, 1181 (1999).
22. B. T. Kelly, *Physics of Graphite* (Applied Science Publishers, London, 1981).
23. J. Goma, A. Oberlin, *Thin Solid Films* **65**, 221 (1980).
24. J. N. Rouzaud, A. Oberlin, C. Beny-Bassez, *Thin Solid Films* **105**, 75 (1983).
25. C. Jin, K. Suenaga, S. Iijima, *Nano Lett.* **8**, 1127 (2008).
26. Y. W. Son, M. L. Cohen, S. G. Louie, *Phys. Rev. Lett.* **97**, 216803 (2006).
27. M. Vandescuren, P. Hermet, V. Meunier, L. Henrard, Ph. Lambin, *Phys. Rev. B* **78**, 195401 (2008).
28. S. Latil, V. Meunier, L. Henrard, *Phys. Rev. B* **76**, 201402 (2007).
29. D. A. Areshkin, D. Gunlycke, C. T. White, *Nano Lett.* **7**, 204 (2007).
30. We thank Z. Ren, S. Chen, B. I. Yakobson, S. Gradecak, G. Dresselhaus, and G. Chen for valuable and fruitful discussions, and E. Gracia-Espino for providing the Pt-coated ribbons that we used in some experiments.

This work was supported by NSF grant Nanoscale Interdisciplinary Research Teams CTS-05-06830. We also thank Consejo Nacional de Ciencia y Tecnología (CONACYT)–Mexico for grants 56787 (Laboratory for Nanoscience and Nanotechnology Research–LINAN), 45772 (M.T.), 41464–Interamerican Collaboration (M.T.), 2004-01-013/SALUD-CONACYT (M.T.), and Ph.D. scholarships (J.C.-D. and J.M.R.-H.). A portion of the present research was supported in part by the Laboratory Directed Research and Development Program of ORNL, managed by UT-Battelle, by the Division of Materials Science and Engineering, U.S. Department of Energy, and by the Center for Nanophase Materials Sciences, sponsored by the Division of Scientific User Facilities, U.S. Department of Energy (V.M. and B.G.S.). A patent that is related to the production of these graphic nanoribbons has been submitted by some of the authors and holds the U.S. patent application number 12/042,544.

Supporting Online Material

www.sciencemag.org/cgi/content/full/323/5922/1701/DC1
Materials and Methods
SOM Text
Figs. S1 to S6
References

6 October 2008; accepted 10 February 2009
10.1126/science.1166862

Graphene at the Edge: Stability and Dynamics

Çağlar Ö. Girit,[1,2] Jannik C. Meyer,[1,2] Rolf Erni,[3] Marta D. Rossell,[3] C. Kisielowski,[3] Li Yang,[1,2] Cheol-Hwan Park,[1,2] M. F. Crommie,[1,2] Marvin L. Cohen,[1,2] Steven G. Louie,[1,2] A. Zettl[1,2]*

Although the physics of materials at surfaces and edges has been extensively studied, the movement of individual atoms at an isolated edge has not been directly observed in real time. With a transmission electron aberration–corrected microscope capable of simultaneous atomic spatial resolution and 1-second temporal resolution, we produced movies of the dynamics of carbon atoms at the edge of a hole in a suspended, single atomic layer of graphene. The rearrangement of bonds and beam-induced ejection of carbon atoms are recorded as the hole grows. We investigated the mechanism of edge reconstruction and demonstrated the stability of the "zigzag" edge configuration. This study of an ideal low-dimensional interface, a hole in graphene, exhibits the complex behavior of atoms at a boundary.

Graphene, a single atomic layer of carbon atoms bonded in a hexagonal lattice, is one of few materials that are stable in two dimensions (*1*) and free-standing when suspended (*2*). This unexpected stability (*3*), combined with its exotic band structure and other unusual physical properties (*4*), has led to a considerable amount of experimental research (*5*–*11*). Of the many theoretical studies of graphene, a substantial portion are devoted to the physics of graphene edges, whose structure in narrow graphene ribbons is predicted to have a major impact on their electronic properties (*12*, *13*). Experimental studies of the graphene edge have lagged behind, mainly due to the difficulty of atomically resolving and characterizing the boundaries of graphene sheets, but would give insight into the one-dimensional (1D) interface of a purely 2D structure.

The traditional method of obtaining atomic resolution on surfaces and edges is scanning tunneling microscopy (STM) or atomic force microscopy (AFM). Although there are several atomically resolved AFM/STM studies of graphene (*14*–*16*), as well as studies of step edges in graphite (*17*), there are several problems in observing dynamics of the edge atoms with scanning probe techniques. First, typical scan speeds are on the order of minutes to hours, which may be too slow to capture the movement of atoms. Second, the highest resolution and stability is obtained at cryogenic temperature, where the dynamics may be frozen out. Finally, the sample is usually on a substrate, which can strongly influence the behavior of atoms both in the bulk and at the edge. To observe dynamics on a time scale of seconds, the only alternative to scanning probe microscopes with comparable spatial resolution is the transmission electron microscope (TEM). Indeed, the dynamics of atom columns composed of heavy atoms were observed in this manner (*18*).

Traditional TEMs lack the necessary resolution at the low operating voltages required to avoid immediate sample damage. Previous 100 to 200 kV TEM studies of few-layer graphitic materials showed that some microscopes have difficulty resolving the lattice and are not capable of atomically resolving edges (*19*–*21*), making image interpretation ambiguous. By using the Transmission Electron Aberration-corrected Microscope monochromated (TEAM 0.5) (*22*), capable of sub-Ångstrom resolution even at 80 kV, we imaged every carbon atom in the lattice of suspended single-layer graphene (*23*). We employed the same microscope to record the dynamics of carbon atoms on the edge of a hole in a graphene sheet. The sample was prepared as described previously (*24*), and details of the microscope configuration can be found in (*23*). The entire experiment was conducted in the high-vacuum environment ($<10^{-7}$ mbar) of the microscope chamber.

Movie S1 shows the evolution of the hole within a suspended graphene sheet. Each frame averages 1 s of exposure, and the frames themselves are 4 s apart. The carbon atoms are shown as white because the spherical aberration was chosen to be negative (*25*). The spatial sampling is 26 ± 4 pm/pixel, determined by fitting for the measured atomic positions and using the known atomic spacing of 1.42 Å. Figure 1A shows the first frame of the sequence. The hole, initially formed through prolonged irradiation by the electron beam, is clearly visible near the center of the frame and is surrounded by the hexagonal carbon lattice. The structures lining the boundary of the frame are adsorbates

[1]Department of Physics, University of California at Berkeley, Berkeley, CA 94720, USA. [2]Materials Sciences Division, Lawrence Berkeley National Laboratory, Berkeley, CA 94720, USA. [3]National Center for Electron Microscopy, Lawrence Berkeley National Laboratory, Berkeley, CA 94720, USA.

*To whom correspondence should be addressed. E-mail: azettl@berkeley.edu